Anticancer effects of the HDAC inhibitor, 3β,6β-dihydroxyurs-12-en-27-oic acid, in MCF-7 breast cancer cells via the inhibition of Akt/mTOR pathways

JONG SEUNG LIM, SO YOUNG KYUNG, YUKYOUNG JEON, IN SU KIM, JONG HWAN KWAK and HYUNG SIK KIM

School of Pharmacy, Sungkyunkwan University, Suwon, Gyeonggi-do 16419, Republic of Korea

Received July 28, 2022; Accepted October 11, 2022

DOI: 10.3892/or.2023.8480

Abstract. *Astilbe chinensis* (*A. chinensis*) is a perennial herb that is used to treat chronic bronchitis and pain. The anticancer activity of 3β,6β-dihydroxyurs-12-en-27-oic acid (ACT-3), a major component isolated from *A. chinensis*, has not yet been investigated in detail. The purpose of the present study was to investigate the histone deacetylase (HDAC) inhibitory and anticancer activities of ACT-3 compared with suberoylanilide hydroxamic acid (SAHA) in MCF-7 human breast cancer cells. The purity of ACT-3 was determined using high-performance liquid chromatography. In the present study, the effects of ACT-3 on anticancer effects of MCF-7 cells were determined by measuring the level of apoptotic cell death and cell cycle regulator using flow cytometry analysis and western blot analysis, respectively. The effects of ACT-3 on HDAC enzyme activity were measured using assay kits. ACT-3 and SAHA increased the levels of acetylated histone H3 and reduced the levels of HDAC1 and HDAC3 in MCF-7 cells. ACT-3 significantly decreased the cell viability in a concentration-dependent manner and induced different morphological changes at high concentrations. ACT-3 and SAHA significantly inhibited the colony formation in MCF-7 cells. ACT-3 inhibited total HDAC activity in a dose-dependent manner. ACT-3 significantly reduced the expression levels of cyclin D1 and cyclin-dependent kinase 4, and upregulated the expression levels of $p21^{WAF1}$ and p53. A significant increase in the G1 phase cell population was observed in MCF-7 cells and ACT-3 induced apoptosis by reducing the ratio of B-cell lymphoma-2 (Bcl-2)/Bcl-2-associated X (Bax) and releasing cleaved caspase 9. Additionally, ACT-3 significantly increased autophagic cell death by inhibiting the serine-threonine kinase/mammalian target of the rapamycin pathway. Autophagy induction was confirmed via acridine orange staining. ACT-3 significantly increased the pERK1/2 and p21 in MCF-7 cells. Thus, the activated ERK pathway played an important role in cell cycle arrest and apoptosis via ERK-dependent induction of p21 in MCF-7 cells. These data indicated that ACT-3 can be used as a promising anticancer agent to overcome the limitations and reduce the side effects of conventional anticancer drugs.

Correspondence to: Professor Hyung Sik Kim or Dr Jong Hwan Kwak, School of Pharmacy, Sungkyunkwan University, 2066 Seobu-Ro, Suwon, Gyeonggi-do 16419, Republic of Korea
E-mail: hkims@skku.edu
E-mail: jhkwak@skku.edu

Key words: breast cancer, 3β,6β-dihydroxyurs-12-en-27-oic acid, *Astilbe chinensis*, HDAC inhibitor, cell cycle, apoptosis, autophagy

Introduction

Histone deacetylase (HDAC) inhibitors are promising anticancer agents for various types of cancer. Recently, an increasing number of structurally diverse HDAC inhibitors, including suberoylanilide hydroxamic acid (SAHA), trapoxin and sodium butyrate, have been reported to be valuable anticancer agents (1-3). HDAC inhibitors belong to a heterogeneous class of compounds, including derivatives of short-chain fatty acids, hydroxamic acids, cyclic tetrapeptides and benzamides (4,5). SAHA is a commonly used potent class I and II HDAC inhibitor. These HDAC inhibitors regulate the expression of target genes involved in cancer cell growth and proliferation (6,7), morphological transformation of oncogenic cells (8), and inhibition of cancer cell invasion and migration (9,10). The potential use of HDAC inhibitors in cancer chemotherapy is currently being investigated in clinical trials, and well-tolerated safety profiles of these drugs have been demonstrated in clinical studies (11).

Breast cancer is the most serious health problem in women worldwide (12). After surgery, chemotherapy with anticancer agents is used for breast cancer treatment. HDAC inhibitors exhibit potent anti-proliferative effects *in vitro* and *in vivo* and interfere with estrogen signaling, regulating estrogen receptor (ER)α and ERβ expression and function (13). HDAC inhibitors induce apoptosis in both ERα-positive and -negative breast tumor cells (14,15). Failure of breast cancer treatment is generally attributed to drug resistance and toxicity. Therefore, effective and safe anticancer agents are required. Medicinal plants have gained attention as effective and value-added sources of anticancer agents (6).

Previously, naturally occurring dietary compounds that inhibit HDAC activity have been shown to exhibit a potent sensitization effect on cancer cells, rendering them susceptible to apoptosis by various anticancer drugs (16,17). In particular, triterpenoids, present in most plants, are mainly used in the medical field (16,17). Previously, certain triterpenoids have been reported to have immunomodulatory and anticancer effects (18). *Astilbe chinensis* (*A. chinensis*) (Maxim.) Franch. & Sav. is a perennial herb of the family *Saxifragaceae* that grows in humid areas of mountains (19). *A. chinensis* is known to cure chronic bronchitis, arthralgia, inflammation-induced pain, headaches and stomachalgia. In addition, previous studies have reported that triterpenoids isolated from *A. chinensis* have *in vitro* cytotoxic effects on various cell lines (20,21). However, the detailed anticancer mechanisms of the isolated compounds remain unknown.

In the present study, 3β,6β-dihydroxyurs-12-en-27-oic acid (ACT-3) was isolated from *A. chinensis* and its anticancer effect was investigated in human breast cancer cells. In the present study, the anticancer activity and cellular mechanism of ACT-3 was established. The results suggested that ACT-3 has the potential to replace or be used in combination with existing anticancer agents for breast cancer therapy.

Materials and methods

Chemicals and reagents. SAHA was purchased from Sigma-Aldrich; Merck KGaA. Dulbecco's modified Eagle's medium (DMEM), fetal bovine serum (FBS), and cell culture supplements were obtained from Gibco; Thermo Fisher Scientific, Inc. Primary antibodies against acetyl-Histone H3 (cat. no. 8848), HDAC1 (cat. no. 34589), HDAC3 (cat. no. 3949), B-cell lymphoma-2 (Bcl-2; cat. no. 15071), Bcl-2 associated X protein (Bax; cat no. 5023), β-actin (cat no. 3700), light chain 3 (LC3; cat no. 3868), beclin-1 (cat. no. 3738), Atg5 (cat. no. 12994), Atg7 (cat. no. 8558), cleaved-poly (ADP-ribose) polymerase (c-PARP; cat. no. 9541), caspase-3 (cat. no. 9662), caspase-8 (cat. no. 9746), caspase-9 (cat. no. 9508), cyclin-dependent kinase 2 (CDK2; cat. no. 2546), CDK4 (cat. no. 12790), p53 (cat. no. 2527), p21 (cat. no. 2947), phosphoinositide 3-kinase (PI3K; cat. no. 4255), phosphorylated (p)-PI3K (cat. no. 4228), Akt (cat. no. 9272), p-Akt (cat. no. 9271), ERK1/2 (cat. no. 9102), p-ERK1/2 (cat. no 9101), mTOR (cat. no. 2972), p-mTOR (cat. no. 2971) and MMP2 (cat. no. 4022), MMP9 (cat. no. 3852), TIMP1 (cat. no. 8946) and TIMP2 (cat. no. 5738) were purchased from Cell Signaling Technology, Inc. Primary antibodies against cyclin A (cat. no. sc-271682), cyclin D1 (cat. no. sc-8396), p27 (cat. no. sc-53871) and horseradish peroxidase-conjugated secondary antibodies (anti-mouse IgG; cat. no. sc-516102 and anti-rabbit IgG; cat. no. sc-2357) were purchased from Santa Cruz Biotechnology, Inc. Immunoblots for total H1 were performed with an anti-H1 antibody (cat. no. ab17584; Abcam). All drugs were dissolved in dimethyl sulfoxide (DMSO) and stored at -20˚C until use. The final concentration of DMSO was less than 0.1% (v/v).

Plant material. Aerial parts of *A. chinensis* were collected in September 2018 at Hambaek mountain (Gangwon, Republic of Korea). A voucher specimen was deposited in the School of Pharmacy of Sungkyunkwan University (SKKU-Ph-18-021).

Extraction and isolation of ACT-3 from A. chinensis. The dried aerial parts of *A. chinensis* (300 g) were extracted twice with methanol (MeOH, 5 l) at room temperature for a day, and once at 60˚C for 5 h. The extracts were then combined and concentrated under reduced pressure at 40˚C. MeOH extract (40.56 g) was suspended in 500 ml distilled water and partitioned with three organic solvents to give dichloromethane (CH_2Cl_2; 8.75 g), ethyl acetate (EtOAc; 5.29 g), n-butanol (n-BuOH; 8.14 g), and water (18.50 g) fractions. The dichloromethane fraction was subjected to column chromatographic separation using silica gel with stepwise elution of hexane-EtOAc (50:1-1:1), hexane-EtOAc-MeOH (10:10:0.5 to 10:10:4) and CH_2Cl_2-MeOH (1:1) to yield 13 fractions (MC-1-MC-13). MC-9 fraction was further chromatographed twice using silica gel (hexane-EtOAc=7:1 and 5:1) to obtain ACT-3. The chemical structure of ACT-3 was identified from spectral data obtained NMR experiments that were performed on Bruker AvanceCore 400 spectrometer and Bruker AVANCE III 700 spectrometer. To determine the purity of ACT-3, high-performance liquid chromatography (HPLC) analysis was carried out on a reversed-phase (RP) C_{18} column and a UV detector using gradient elution. HPLC analysis was performed using a Knauer HPLC system consisting of a Manager 5000, two Pumps 1,000, a UV Detector 2500, and a Kinetex (Phenomenex) 5-μm C18 100 Å column (150x4.6 mm). The eluent consisted of (A) acetonitrile and (B) water. The gradient profile was as follows: 0-3 min, isocratic elution with 43% A in B; 3-20 min, linear change from 43-80% A in B; 20-30 min, linear change from 80-100% A in B. The flow rate and column oven temperature were set to 1.0 ml/min and 40˚C, respectively. The UV absorption was measured at a wavelength of 210 nm.

HDAC enzyme activity assay. To assess the HDAC inhibitory potency of ACT-3, commercially available HeLa cell nuclear extracts were treated with ACT-3 (2, 4 and 8 μM). Total HDAC activity was measured using the SensoLyte 520 fluorometric HDAC Activity Assay kit (AnaSpec), according to the manufacturer's instructions. Suramin (10 and 20 μM) and SAHA (5 μM) were used as reference compounds. Briefly, HDAC enzyme was incubated with the vehicle or various concentrations of suramin and SAHA at 37˚C for 30 min in the presence of an HDAC fluorometric substrate (22). The HDAC assay developer (which produces a fluorophore in the reaction mixture) was added, and fluorescence was measured using VICTOR 3 (Perkin Elmer, Inc.) with excitation at 490 nm and emission at 520 nm. The activities were calculated using GraphPad Prism (GraphPad Software, Inc.).

Cytotoxicity assay. Human breast cancer MCF-7 cells were purchased from the American Type Culture Collection. MCF-7 cells were cultured in DMEM supplemented with 10% FBS, streptomycin (100 μg/ml) and penicillin (100 U/ml). Cells were maintained as monolayers and incubated at 37˚C in a humidified atmosphere containing 5% CO_2. Cytotoxicity was assessed using 3-(4,5-dimethylthiazol-2-yl)-2,5-diphenyl-tetra-zolium bromide (MTT; 5 mg/ml; Sigma-Aldrich). Cells were seeded into a 96-well plate at a density of $7x10^3$ cells/well. After incubation at 37˚C for 24 h, cells were treated with ACT-3 (3.125-50 μM) and SAHA (5 μM) for 48 h. After incubation, 15 μl of the MTT reagent was loaded into each

well, and the plates were incubated at 37˚C for 4 h in the dark. The supernatant of each well was aspirated and formazan crystals were dissolved in 100 μl DMSO at 37˚C for 15 min with gentle agitation. A VERSA MAX Microplate Reader (Molecular Devices Corp.) was used to measure the absorbance of each well at 540 nm wavelength. Three independent experiments were performed for each condition. The median inhibitory concentration (IC_{50}) values were calculated from the sigmoidal concentration-response using the GraphPad Prism software (version 5.0 for Windows) statistical software package (GraphPad Software, Inc.).

Colony formation assay. The colony formation assay was performed as previously described (23). Cells (1,000 cells per well) seeded in a six-well plate were cultured for 10 days and treated with various concentrations of either ACT-3 or SAHA for 14 days until the appearance of colonies. The culture medium was replaced with fresh medium every two days. Cells were fixed with 4% paraformaldehyde at room temperature for 30 min, followed by staining with 0.05% crystal violet, and incubated at 37˚C for 15 min. Colonies containing more than 20 cells were counted.

Cell cycle analysis. The cells were treated with ACT-3 (2, 4 and 8 μM) and SAHA (5 μM) for 48 h. Suspended or adhered cells were harvested separately. The cells ($1x10^6$) were washed with 1% bovine serum albumin (Sigma-Aldrich; Merck KGaA), fixed in chilled 95% ethanol, and stained with cold propidium iodide (PI) solution (10 μg/ml PI and 100 μg/ml RNase in phosphate-buffered saline (PBS) in the dark for 30 min at room temperature. Data acquisition and analysis were performed using a flow cytometry system (BD Accuri C6; Cytometers, Inc.).

Evaluation of apoptosis. The Annexin V-FITC binding assay was performed using Annexin V-FITC detection kit I (BD Biosciences), according to the manufacturer's instructions. The cells were treated with ACT-3 and SAHA for 48 h. Cells were counted after trypsinization and washed twice with cold PBS. The cell pellet was resuspended in 100 μl binding buffer at a density of $1x10^3$ cells/ml and incubated with 5 μl FITC-conjugated Annexin-V and 5 μl PI for 15 min at room temperature in the dark. A total of 400 μl of 1X binding buffer were added to each sample tube, and the samples were immediately analyzed via flow cytometry (Accuri Cytometers, Inc.).

Western blot analysis. Cells were treated with ACT-3 and SAHA for 48 h, harvested via trypsinization, and washed twice with cold PBS. For total protein isolation, the cells were suspended in PRO-PREP protein extract solution (Intron Biotechnology, Inc.). Protein concentrations were measured using a protein assay kit (cat. no. 5000002; Bio-Rad Laboratories, Inc.), according to the manufacturer's instructions. The cell extract with 20 μg protein was loaded onto 6-15% sodium dodecyl sulfate-polyacrylamide gels. After electrophoresis, proteins were transferred onto polyvinylidene difluoride (PVDF) membranes (Millipore Sigma). The membranes were incubated for 1 h in TNA (10 mM Tris-Cl, pH-7.6, 100 mM NaCl, and 0.5% Tween 20) buffer containing 5% skim milk. Membranes were then incubated with primary antibodies (1:200 or 1:250) overnight at 4˚C. After washing for 1 h with TNA buffer, the membranes were incubated with horseradish peroxidase-conjugated anti-mouse (1:10,000) or anti-rabbit antibodies (1:10,000) for 30 min at room temperature. The blots were developed using an enhanced chemiluminescence (ECL)-plus kit (Amersham; Cytiva). Using the ImageJ software (1.52v; National Institutes of Health), the band intensities were densitometrically quantified.

Acridine orange staining. Cells were cultured in cover-glass bottom dish at a density of $1x10^5$ cells per dish, cultured for 24 h, and incubated with the indicated drug in DMEM containing 1% FBS for 48 h. The medium was removed, and the cells were stained with acridine orange (1 μg/ml) at 37˚C for 15 min. After removing the staining solution, PBS was added to the dish and the cells were examined under a fluorescence microscope at x600 magnification (FV10i; Olympus Corporation).

Wound-healing assay. MCF-7 cells ($3x10^4$ cells/well) were seeded into a 24-well plate in media containing 10% FBS and incubated at 37˚C for 24 h. After incubation, scratches were introduced using a wound maker (Essen Bioscience) and the indicated concentrations of ACT-3 (2, 4 and 8 μM) or SAHA (1 μM) were used to treat the cells for seven days. The culture medium was replaced with fresh culture medium containing ACT-3 or SAHA every two days. Then, the cells were washed twice with PBS and the wound images were obtained daily using IncuCyte ZOOM (Sartorius AG), and scratch density was determined using the IncuCyte software (v2019B; Satorius AG).

Statistical analysis. Data are expressed as the mean ± SD of at least three independent experiments. Statistical analysis was performed using one-way analysis of variance, followed by Bonferroni's multiple comparison tests. $P<0.05$ was considered to indicate a statistically significant difference. All statistical comparisons were performed using the SigmaPlot software and Statistical Package for the Social Sciences v.13 (SPSS, Inc.).

Results

Isolation and characterization of ACT-3. ACT-3, an ursane-type triterpene, was isolated from the aerial part of A. chinensis and identified as 3β,6β-dihydroxyurs-12-en-27-oic acid (Fig. 1A) by comparing its spectral data (Fig. 1B and C) with literature values (21). The purity of ACT-3 was determined to be 98.3% by HPLC analysis using RP C_{18} column and UV detector (Fig. 1D).

ACT-3 inhibits the activity and expression of HDAC in MCF-7 cells. The effect of ACT-3 on total HDAC enzyme activity was measured. As revealed in Fig. 2A, ACT-3 significantly inhibited the total HDAC enzyme activity in a concentration-dependent manner. The potency of the enzyme activity was similar to that of SAHA. In addition, the effects of ACT-3 and SAHA on the expression levels of acetylated H3 and HDAC1/3 were examined in MCF-7 cells. ACT-3 significantly increased acetylated H3 expression at sub-micromolar concentrations. Similar to SAHA, ACT-3 significantly reduced the expression levels of HDAC1/3

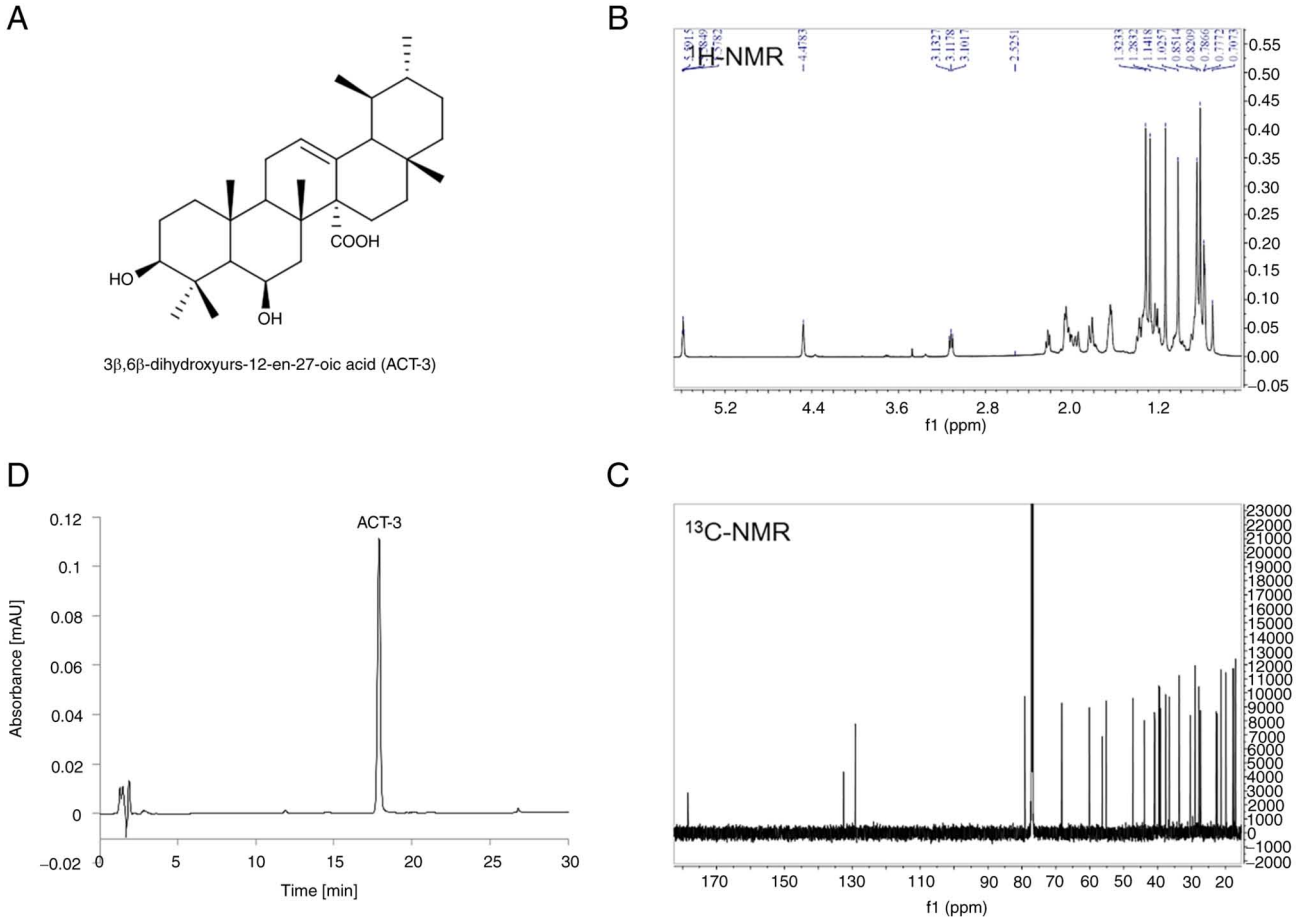

Figure 1. Characterization of (ACT-3) using NMR spectroscopy and HPLC. (A) Chemical structure of ACT-3. (B) ^{1}H-NMR spectrum of ACT-3 ($CDCl_3$, 400 MHz). (C) ^{13}C-NMR spectrum of ACT-3 ($CDCl_3$, 213 MHz). (D) HPLC-UV chromatogram of ACT-3. HPLC analysis was carried out via gradient elution on a Phenomenex Kinetex C18 column (150x4.6 mm, 5 μm) and UV detector (210 nm). The flow rate and column oven temperature were set at 1.0 ml/min and 40˚C, respectively. ACT-3, 3β,6β-dihydroxyurs-12-en-27-oic acid; NMR, nuclear magnetic resonance; HPLC, high-performance liquid chromatography.

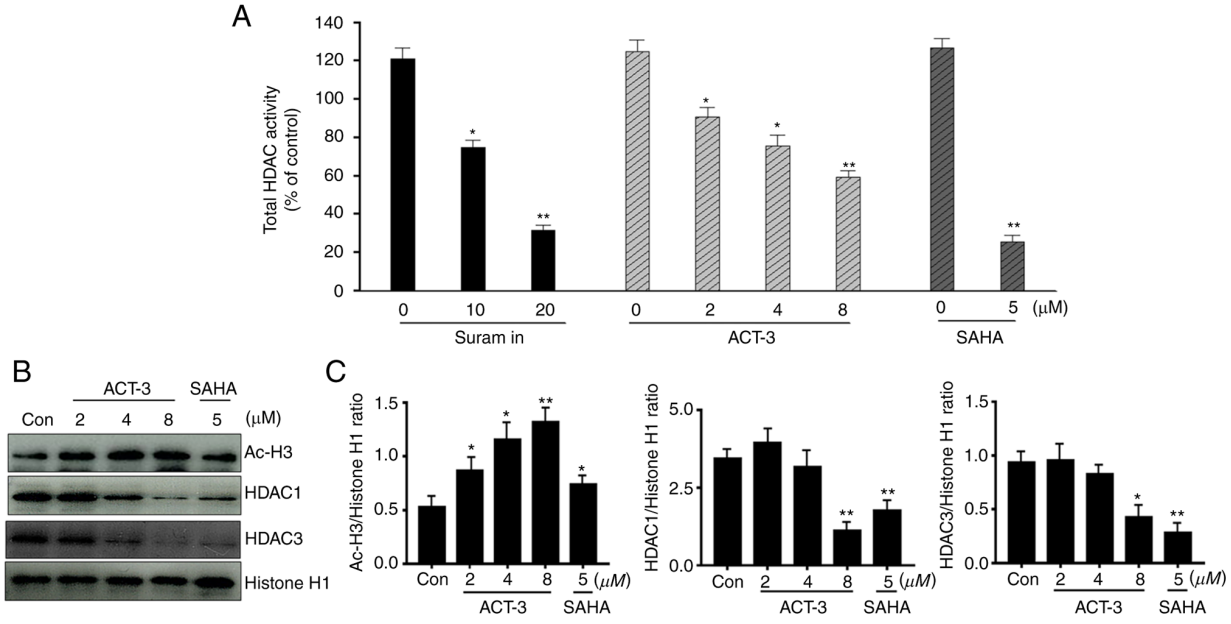

Figure 2. Effect of ACT-3 on HDAC expression levels in MCF-7 cells. (A) Effects of ACT-3, suramin, and SAHA on total HDAC enzyme activity. HDAC enzyme activity was measured using the SensoLyte 520 FRET total HDAC assay kit. (B and C) MCF-7 cells were treated with ACT-3 and SAHA for 48 h and expression levels of Ac-H3, HDAC1, HDAC3 and Histone H1 were analyzed via western blotting. The data are expressed as the mean ± SD of duplicate experiments. Statistical analysis was performed using one-way analysis of the variance (ANOVA), followed by Bonferroni's multiple comparison tests. *P<0.05 and **P<0.01 vs. the control. ACT-3, 3β,6β-dihydroxyurs-12-en-27-oic acid; HDAC, histone deacetylase; SAHA, suberoylanilide hydroxamic acid; Ac-H3, acetylated histone 3.

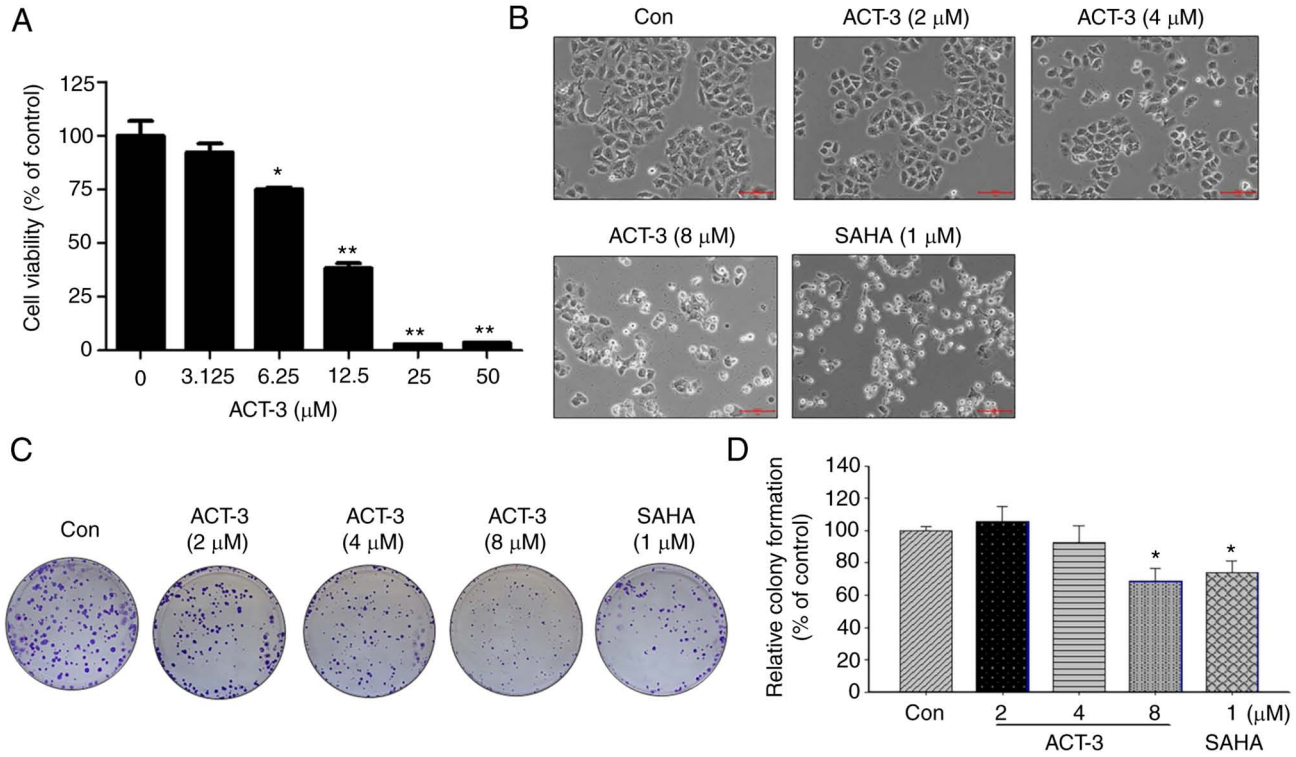

Figure 3. Effect of ACT-3 on the proliferation of MCF-7 breast cancer cells. (A) Cytotoxicity of ACT-3 against the MCF-7 cell lines. Cells were treated with ACT-3 at various concentrations (3.125-50 μM) for 48 h. Cell viability was assessed using the 3-(4,5-dimethylthiazol-2-yl)-2,5-diphenyltetrazolium bromide (MTT) assay. (B) Morphological changes, cell body shrinkage and reduction of cell number in MCF-7 cell lines after ACT-3 (2, 4 and 8 μM) or SAHA (1 μM) treatment for 48 h. (C) Representative images of colony formation assay of MCF-7 cells treated with the indicated concentrations of ACT-3 and SAHA in a six-well plate. (D) Quantitative analysis of colony formation assay of MCF-7 cells treated with the indicated concentrations of ACT-3 and SAHA in a six-well plate. Colony areas were measured using image analyzer. *P<0.05 and **P<0.01. ACT-3, 3β,6β-dihydroxyurs-12-en-27-oic acid; SAHA, suberoylanilide hydroxamic acid.

in MCF-7 cells (Fig. 2B and C). The cytotoxicity of ACT-3 on the normal rat tubular epithelial cell line NRK-52E was also determined. ACT-3 showed a less potent cytotoxicity against normal cells compared with the MDA-MB-231 cells (Fig. S1).

Cytotoxicity of ACT-3 in MCF-7 cells. To investigate the anticancer activity of ACT-3 in MCF-7 breast cancer cells, cell viability was measured using an MTT assay. ACT-3 significantly reduced the viability of MCF-7 cells in a concentration-dependent manner (Fig. 3A). The IC_{50} value of ACT-3 in MCF-7 cells was 8.25 μM. The morphological change in MCF-7 cells induced by ACT-3 treatment resulted in cell shrinkage and increased suspended cell population. Similar morphological changes in MCF-7 cells were observed following SAHA treatment (Fig. 3B). To demonstrate the anticancer effects of ACT-3, a colony formation assay was performed. As revealed in Fig. 3C and D, colony formation by MCF-7 cells was significantly inhibited following treatment with ACT-3 and SAHA.

ACT-3 induces cell cycle arrest in G0/G1 phase in MCF-7 cells. HDAC inhibitors significantly block the proliferation of various cancer cells via cell cycle arrest at a specific phase (24,25). To confirm the anticancer effect of ACT-3, cell cycle was analyzed in MCF-7 cells treated with ACT-3 (2, 4 or 8 μM) and SAHA (5 μM) for 48 h. As demonstrated in Fig. 4A, ACT-3 induced G0/G1 phase cell cycle arrest in a concentration-dependent manner. However, SAHA (5 μM) increased the G2/M phase cell accumulation to 59.99% compared with that in the control (32.01%). To evaluate the effect of ACT-3 on the expression levels of cell cycle regulators, the expression of cyclins and CDK levels were determined. ACT-3 significantly reduced the expression levels of cyclin D1, CDK4 and CDK2. Furthermore, ACT-3 significantly increased p27 and p21 expression at a high concentration (8 μM) in MCF-7 cells (Fig. 4B and C).

ACT-3 induces apoptotic cell death in MCF-7 cells. To evaluate the apoptotic cell death in MCF-7 cells after ACT-3 treatment, annexin V-FITC-conjugated staining and western blot analysis were performed. Despite the pronounced concentration-dependent cell death observed in the cytotoxicity assay, only a small change in apoptotic cell death was detected at the highest ACT-3 concentration (Fig. 5A). A significant increase in Bax and simultaneous decrease in Bcl-2 expression levels were observed following ACT-3 treatment (Fig. 5B and C). Moreover, there was a significant increase in the expression levels of c-PARP in MCF-7 cells following ACT-3 (8 μM) and SAHA treatment (Fig. 5B). However, p53 expression was not changed in MCF-7 cells by ACT-3 and SAHA treatment (Fig. 5B).

ACT-3 induces autophagic cell death in MCF-7 cells. To elucidate ACT-mediated autophagic cell death by ACT-3, firstly acridine orange staining was performed. Acridine orange is

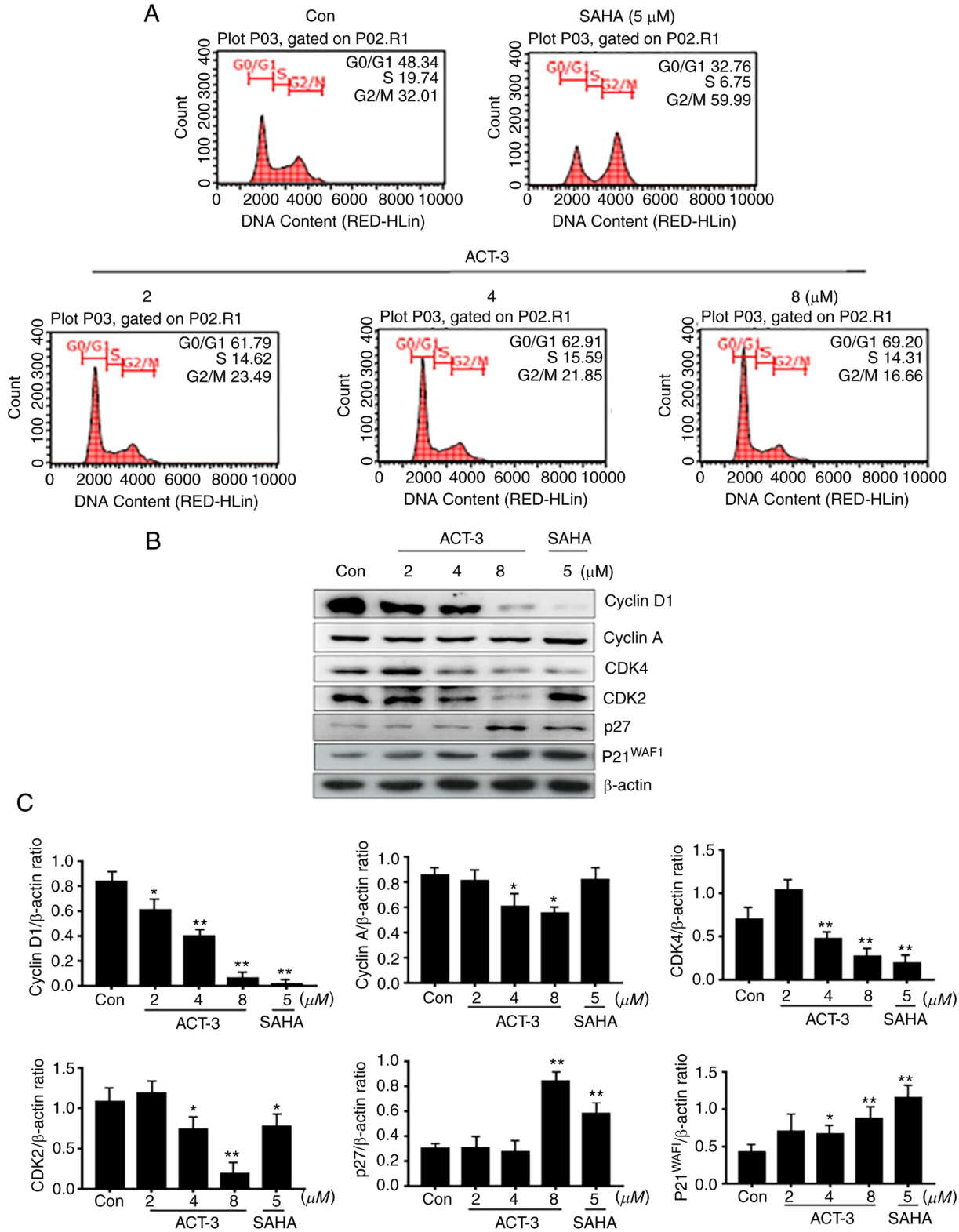

Figure 4. Effect of ACT-3 on the cell cycle distribution in MCF-7 cell lines. (A) Cells were treated with the indicated concentrations of ACT-3 and SAHA for 48 h, stained with propidium iodide (PI) and analyzed via flow cytometry to determine the cell cycle distribution. (B and C) Cells were treated with the vehicle control, ACT-3 (2, 4 and 8 μM), or SAHA (5 μM) for 48 h and the expression levels of cell cycle distribution-related proteins were determined via western blotting. β-actin was used as a loading control. The data are expressed as the mean ± SD of duplicate experiments. Statistical analysis was performed using one-way analysis of the variance (ANOVA), followed by Bonferroni's multiple comparison tests. *P<0.05 and **P<0.01 vs. the control. ACT-3, 3β,6β-dihydroxyurs-12-en-27-oic acid; SAHA, suberoylanilide hydroxamic acid.

a fluorescent dye that accumulates in acidic cellular compartments in a pH-dependent manner. Under neutral conditions, the dye emits a green light. However, within acidic vesicles, the dye changes to bright red (26). With acridine orange staining, the control cells and 2-μM ACT-3 showed almost undetectable red fluorescence, indicating the lack of acidic vacuoles

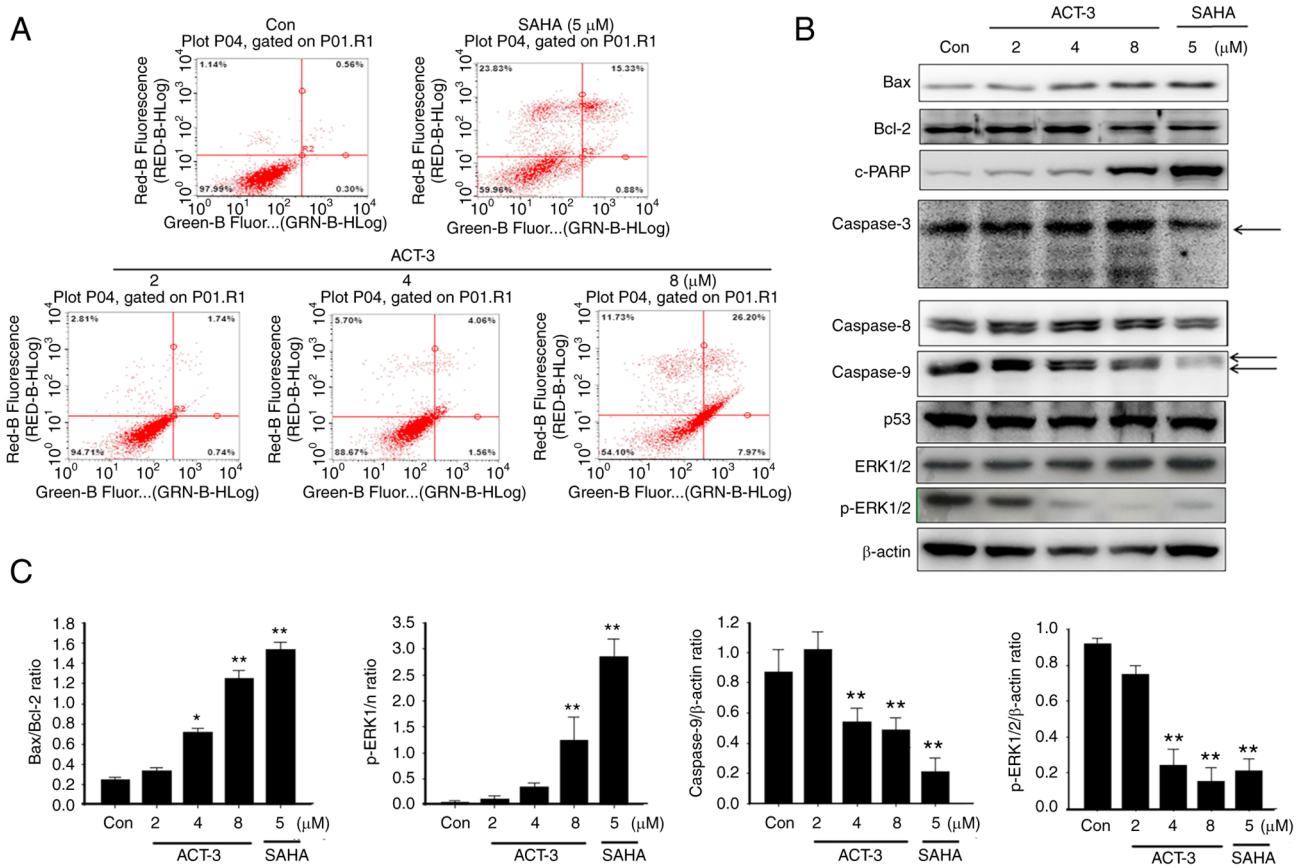

Figure 5. Effect of ACT-3 on apoptotic cell death in MCF-7 cell lines. (A) Cells were treated with the indicated concentrations of ACT-3 and SAHA for 48 h. The flow cytometry profile represents Annexin V-FITC staining on the x-axis and PI staining on the y-axis. (B and C) Cells were treated with the vehicle control, ACT-3 (2, 4, and 8 μM), or SAHA (5 μM) for 48 h and the expression levels of apoptosis-related proteins were determined via western blotting. β-actin was used as a loading control. The data are expressed as the mean ± SD of duplicate experiments. Statistical analysis was performed using one-way analysis of the variance (ANOVA), followed by Bonferroni's multiple comparison tests. *P<0.05 and **P<0.01 vs. the control. ACT-3, 3β,6β-dihydroxyurs-12-en-27-oic acid; SAHA, suberoylanilide hydroxamic acid; p-, phosphorylated.

(AVOs). However, accumulation of red fluorescence was observed with 8 μM ACT-3 and SAHA, indicating the presence of numerous AVOs. Similarly, AVOs were analyzed with acridine orange in the merged figures (Fig. 6A). To evaluate autophagic proteins, their expression levels were determined using western blotting. The levels of LC3-II, a marker of autophagosomes, were significantly increased after treatment with ACT-3 and SAHA-treated cells. The levels of beclin-1 and Atg7 were increased, but Atg5 did not show any changes (Fig. 6B and C). Previous studies have indicated that a majority of anticancer agents suppress the PI3K/mTOR/Akt pathway, which is related to cell proliferation (27). To evaluate the effect of ACT-3 on the PI3K/mTOR/Akt pathway, protein expression levels were evaluated using western blotting. The expression of p-PI3K, PI3K, p-mTOR and p-Akt levels were decreased after ACT-3 treatment in MCF-7 cells (Fig. 6D and E). However, the p-PI3K/PI3K ratio remained unchanged. These results suggested that ACT-3 only downregulates the mTOR/Akt pathway.

ACT-3 inhibits MCF-7 cell migration. To investigate the effects of ACT-3 on the inhibition of MCF-7 cell migration, a wound-healing assay was performed in response to the mechanical scratch wound in the absence or presence of ACT-3 and SAHA. Images of scratch areas from 0-6 days are illustrated. The representative control at each time point is revealed in Fig. 7A, indicating that the scratch was half-closed within three days and completely closed after six days. The percentage of open wound area was determined to quantify the effects of the putative migration inhibitors (Fig. 7B). The present data clearly indicated that treatment with ACT-3 significantly inhibited the cell migration in a concentration-dependent manner. These results suggested that ACT-3 may be an effective inhibitor of MCF-7 breast cancer cell migration. Moreover, the levels of matrix metalloproteinase (MMP)-2 and MMP9 were reduced after treatment with ACT-3 in a concentration-dependent manner. However, ACT-3 did not alter the expression levels of tissue inhibitor of metalloproteinase (TIMP)-1 or TIMP2 (Fig. 7C and D).

ACT-3 shows synergistic anticancer activity with microtubule inhibitors in MCF-7 cells. To investigate the combined effect of ACT-3 and vincristine, the cytotoxicity of MCF-7 cells was measured using the MTT assay with the indicated concentrations of drugs. ACT-3 showed potent cytotoxicity at 6 μM, and vincristine at 5 μM. Combination treatment with ACT-3 (6 μM) and vincristine (5 μM) significantly increased the cytotoxic activity against MCF-7 cells compared with that of the single treatment (Fig. 8A). To evaluate the synergism between apoptotic and autophagic cell death, the expression levels of

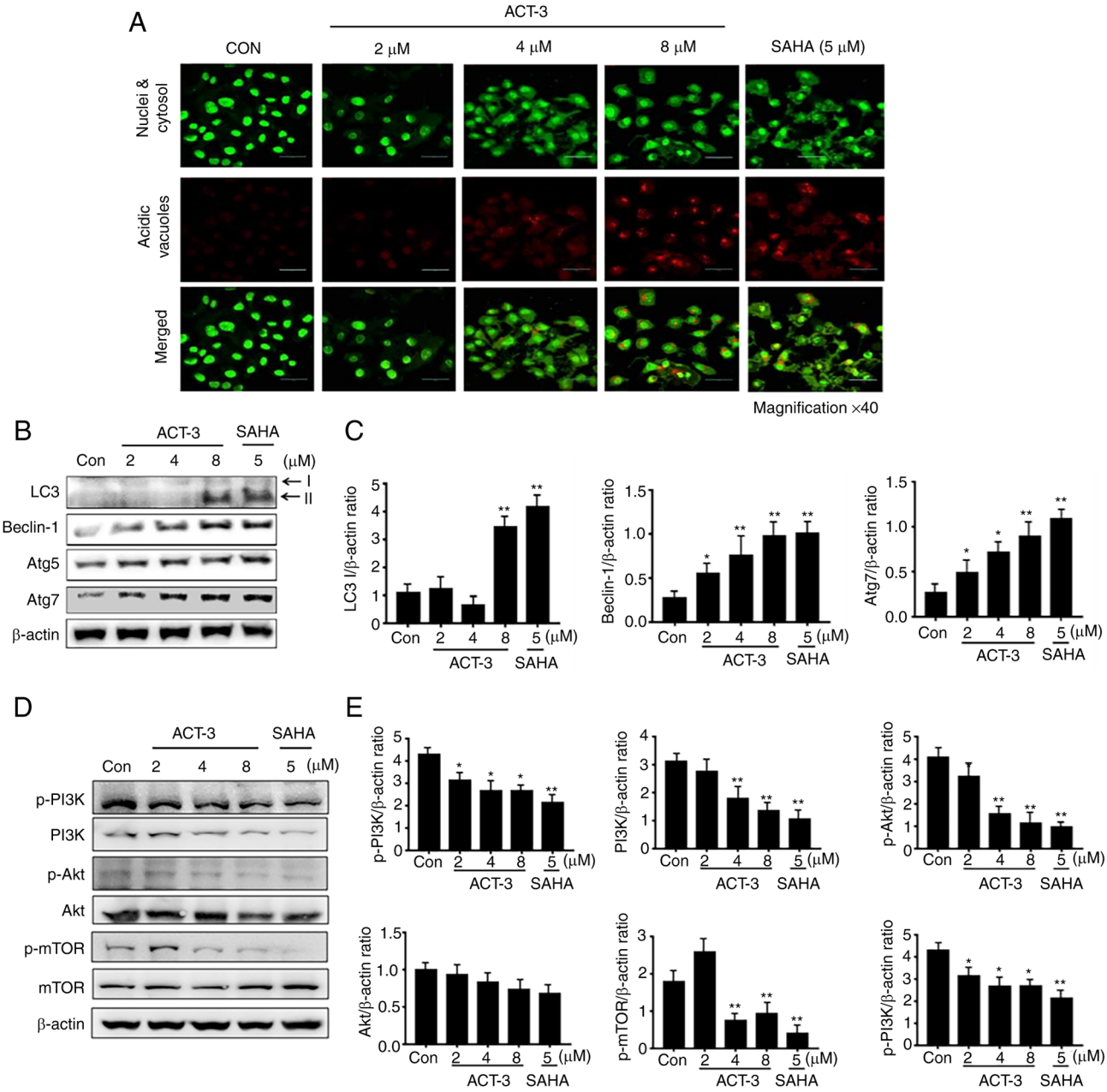

Figure 6. Effects of ACT-3 on autophagy and its related pathways. (A) Immunofluorescence microscopy of acridine orange-stained MCF-7 cell lines treated with indicated concentrations of ACT-3. Images were observed using the confocal laser scanning microscope (LSM 510; magnification, x400). Scale bar, 10 μm. (B and C) Cells were treated with indicated concentrations for 48 h and the expression levels of autophagy-related proteins were determined via western blotting. β-actin was used as a loading control. (D and E) Cells were treated with indicated concentrations for 48 h and the PI3K/Akt/mTOR pathway was analyzed via western blotting. β-actin was used as a loading control. (D) The data are expressed as the mean ± SD of duplicate experiments. Statistical analysis was performed using one-way analysis of the variance (ANOVA), followed by Bonferroni's multiple comparison tests. *P<0.05 and **P<0.01 vs. the control. ACT-3, 3β,6β-dihydroxyurs-12-en-27-oic acid; SAHA, suberoylanilide hydroxamic acid; p-, phosphorylated; LC3, light chain 3.

proteins related to apoptosis and autophagy were evaluated via western blotting. Bax levels were almost unchanged, but Bcl-2 levels were significantly reduced by the combination treatment (Fig. 8B and D). Caspase 3 levels were also decreased by the combination treatment, while cleaved caspase-3 levels were increased (Fig. 8B and D). c-PARP and p53 levels were significantly increased by the combination treatment (Fig. 8B and D). The expression levels of the autophagy-related proteins, Atg5 and Atg7, were not altered (Fig. 8C and D). However, LC3-II protein levels were significantly increased by the combination treatment (Fig. 8C and D). These results indicated that the combination therapy with ACT-3 and vincristine is effective against MCF-7 breast cancer cells.

Discussion

Previously, much attention was paid to the use of HDAC inhibitors as anticancer agents since they can induce either apoptosis or autophagic cell death (22,28,29). In the present study, it was found that ACT-3 induces apoptosis in MCF-7 cells through cell cycle arrest at the G2/M phase. Similar to other HDAC inhibitors, ACT-3 effectively blocked the deacetylation of histone H3

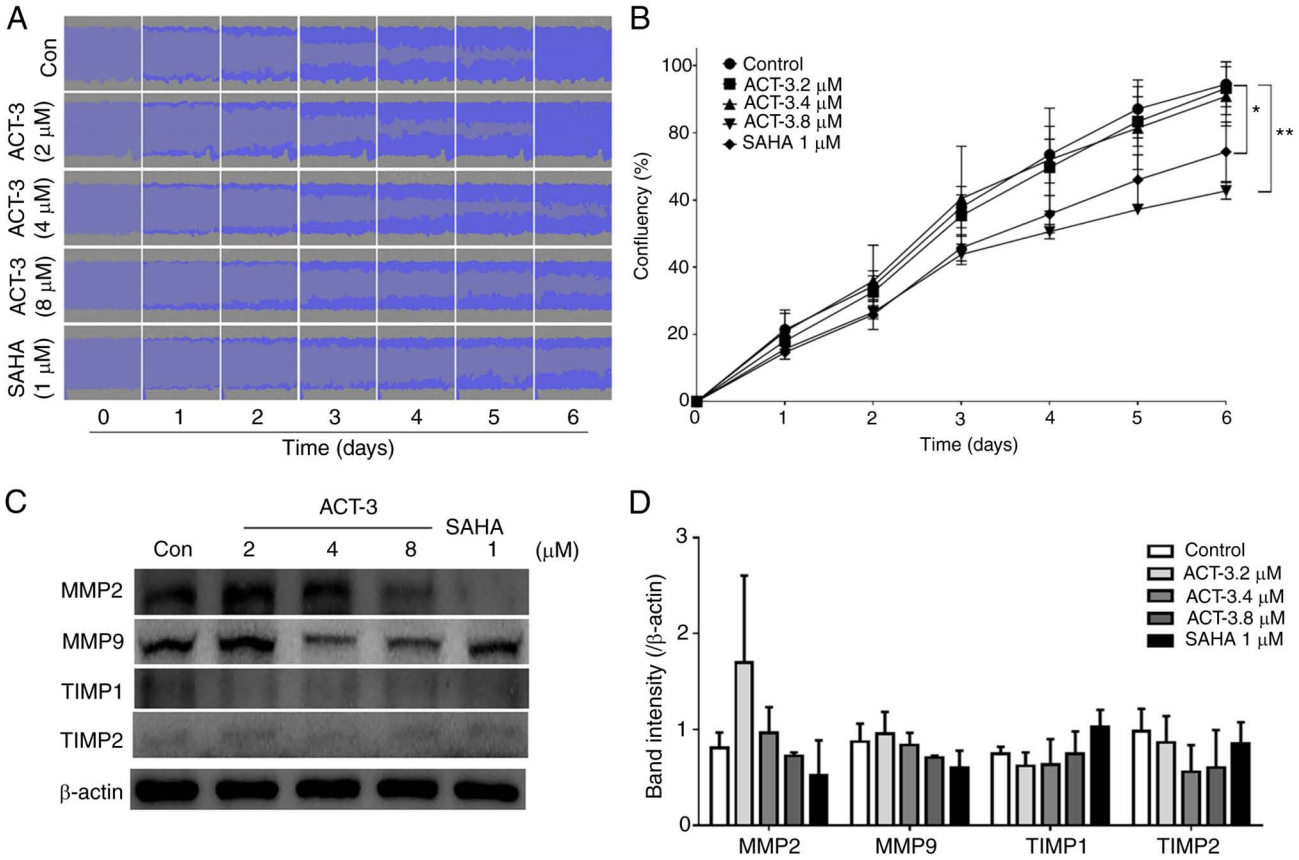

Figure 7. Effect of ACT-3 on MCF-7 cell migration. (A and B) MCF-7 cells were treated with the indicated concentrations of ACT-3 and SAHA. Wound images were obtained daily using IncuCyte ZOOM and scratch density was determined by using IncuCyte software. Statistical analysis was performed using one-way analysis of the variance (ANOVA), followed by Bonferroni's multiple comparison tests. *P<0.05 and **P<0.01 vs. the control. (C and D) Cells were treated with the indicated concentrations of ACT-3 and SAHA. The expression levels of cell migration-related proteins were determined via western blotting. β-actin was used as a loading control. ACT-3, 3β,6β-dihydroxyurs-12-en-27-oic acid; SAHA, suberoylanilide hydroxamic acid; TIMP, tissue inhibitor of metalloproteinase.

and H4 proteins as well as HDAC1/2 expression, which influenced the expression of key target genes that regulate oncogenic pathways and inhibit the expression of cell cycle regulators.

Previous studies have indicated that natural products of *A. chinensis* exhibit hepatoprotective, anti-obesity, anticancer and anti-inflammatory activities. The major mechanism of this anti-inflammatory effect is closely associated with the inhibition of NF-κB activation (30-32). In addition, the extracts or fractions of *A. chinensis* exhibit anticancer activity via the activation of apoptosis by ROS production (33). However, the anticancer activity of the major components isolated from *A. chinensis* has not been clearly investigated. Thus, the major components of *A. chinensis* were isolated using solvent extraction and HPLC and it was found that the most active component was triterpenoid, which also exhibited a potent HDAC enzyme inhibitor. In the present study, ACT-3 showed potent cytotoxicity against MCF-7 cells and the cytotoxicity results were confirmed by cell morphological analysis compared with SAHA, a reference HDAC inhibitor. Previously, a number of studies reported cell shrinkage and that the cells were smaller than before, the cytoplasm was dense, and other organelles were packed during early apoptosis (34,35).

In the present study, a series of experiments were performed to detect the effects of ACT-3 on cancer cell proliferation and migration *in vitro*. The results showed that ACT-3 exhibited cytotoxicity against MCF-7 cells, with an IC_{50} value of 8 μM. The wound-healing assay indicated that MCF-7 cells showed inhibition of migration after treatment with ACT-3. Furthermore, subsequent mechanistic investigation revealed that ACT-3 induced apoptosis and arrested the MCF-7 cell cycle at the G0/G1 stage to exert cytotoxic effects. The expression levels of representative proteins associated with apoptosis were also examined. The proteins of the Bcl-2 family play a vital role in the mitochondria-mediated apoptosis pathway. In the present study, the inhibition of Bcl-2 expression and the increase in Bax protein levels by ACT-3 demonstrated that the compound could promote apoptosis by targeting the mitochondrial pathway. Generally, regulation of the cell cycle plays a vital role in cell growth in a rapidly changing microenvironment (36). During the cell cycle, cyclins and CDKs bind together and successfully perform their roles to regulate the cell cycle. After CDKs bind to cyclins, they activate or inactivate target proteins to enter the next phase of the cell cycle (37-39). In the case of ACT-3, cyclin D1, cdc2 and CDK2 expression levels were inhibited. Cyclin D1 and cdc2 inhibition may suppress the entry of the G0 phase to the G1 phase and exit the G2/M phase. Thus, ACT-3 arrested cells that entered the cell cycle in the G1 phase by inhibiting CDK2. In SAHA, CDK2 was activated. This difference caused the SAHA-treated group to pass the S phase, and the inhibition

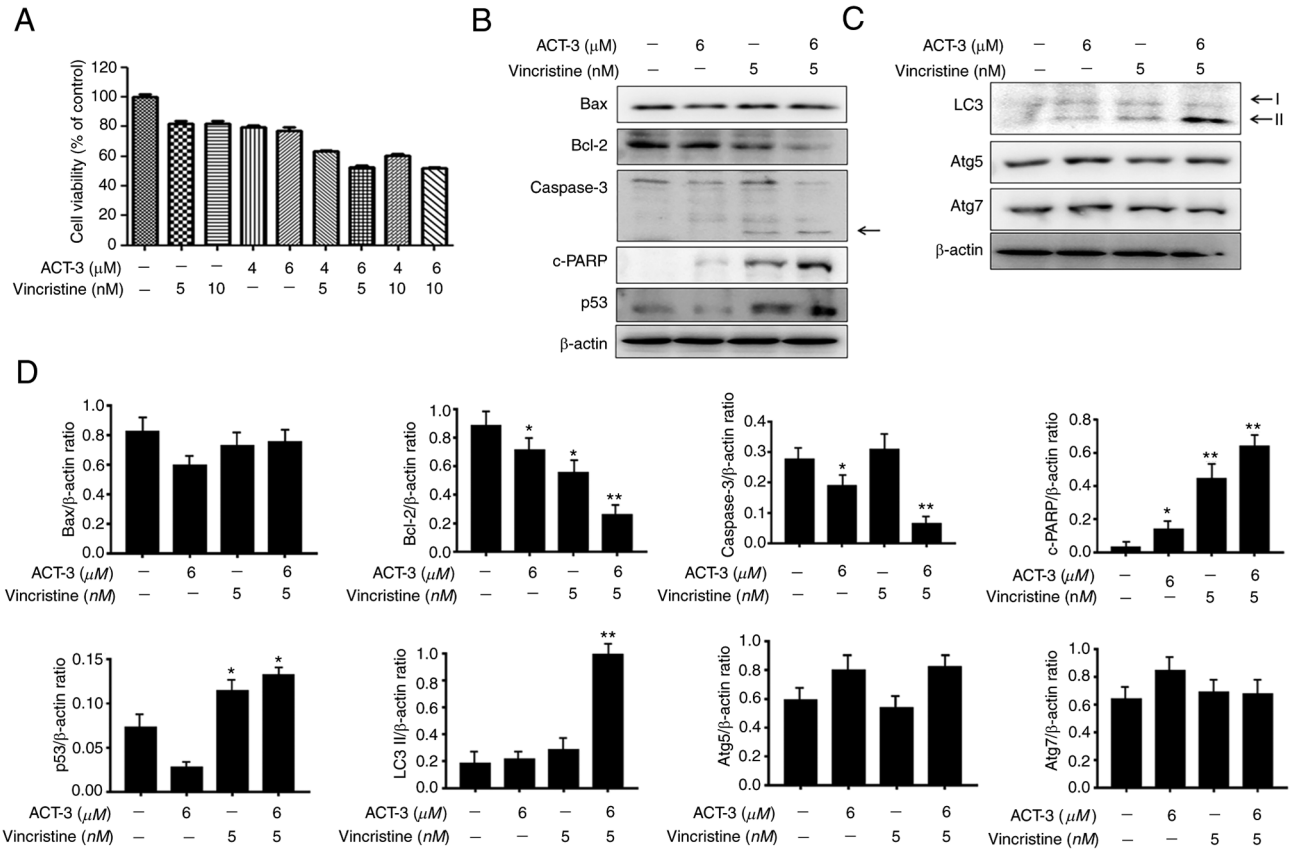

Figure 8. Combined effects of the co-treatment of ACT-3 and vincristine in the MCF-7 cell lines. (A) Synergetic cytotoxic effects of ACT-3 and vincristine. Cells were treated with the indicated concentrations of ACT-3 and vincristine for 48 h. Cell viability was assessed via the MTT assay. (B) Western blot analysis of apoptosis-related proteins. Cells were co-treated with the indicated concentrations of ACT-3 and vincristine for 48 h. β-actin was used as a loading control. (C) Western blot analysis of autophagy-related proteins. Cells were co-treated with the indicated concentrations of ACT-3 and vincristine for 48 h. β-actin was used as a loading control. (D) Densitometric analysis of western blot bands in panels B and C. The data are expressed as the mean ± SD of duplicate experiments. Statistical analysis was performed using one-way analysis of the variance (ANOVA), followed by Bonferroni's multiple comparison tests. *P<0.05 and **P<0.01. ACT-3, 3β,6β-dihydroxyurs-12-en-27-oic acid; LC3, light chain 3; c-, cleaved.

of cyclin B1 and cdc2 prevented entry into mitosis, resulting in arrest in the G2/M phase. To control cell cycle progression, cells generate CDK inhibitors, including protein/kinase inhibitory protein (CIP/KIP), p21 and p27. These proteins are primarily activated by p53, which is triggered by DNA damage (40,41). In the case of ACT-3, increased protein levels of p53 and p27 have been observed to regulate the cell cycle.

Numerous anticancer drugs exert their effects through apoptosis and autophagy after cell growth stops (42). Apoptosis was also analyzed to elucidate the underlying anticancer mechanism. Apoptotic cells have several features including DNA breakdown, protein cross-linking and protein cleavage (43). In the case of ACT-3, the levels of intrinsic-related caspases 3 and 9 slightly decreased in a dose-dependent manner. In fact, tumor cells acquire resistance to apoptosis by overexpression of the anti-apoptotic protein Bcl-2 or the apoptotic protein Bax. Both Bcl-2 and Bax are regulated by p53, a tumor suppressor gene (44,45). p53 induced by DNA damage can maintain the cell cycle. If DNA damage is irreversible, p53 mediates apoptosis (46). ACT-3 inhibits this evasion mechanism by increasing the expression level of Bax and decreasing the expression level of Bcl-2. PARP-1 is a nuclear enzyme that responds to DNA damage and is essential for the maintenance of gene integrity. When DNA damage begins, PARP-1 is proteolyzed by caspases to a DNA-binding domain and formed c-PARP-1 (47). ACT-3 increased PARP-1 activity, which was confirmed by the increased expression level of c-PARP.

Autophagy is a self-degradable process that plays a critical role in balancing cellular environmental homeostasis (48). Autophagy can be activated by various stress conditions such as radiotherapy or chemotherapy, nutrient shortage and cellular damage by intrinsic or extrinsic stress (49,50). Responding to the various stress conditions, expression level of autophagy-related proteins including microtubule-associated protein LC3, beclin-1 and p62 is increased. LC3 is cleaved by ATG4. LC3 combined with phosphatidylethanolamine by ATG3/7 induces a change from the cytosolic form (LC3-I) to the membrane-bound form (LC3-II) (51). Western blot analysis and acridine orange staining showed that LC3-II was increased in 8 μM concentration ACT-3 and SAHA cells. The increased expression of Beclin-1 also confirmed the activation of autophagy. Autophagy is affected by various signaling pathways. First, the protein expression levels of mTOR kinase, which plays a crucial role in cellular growth and protein synthesis, were investigated. Autophagy activation is initiated by decreasing the activity of mTOR, which is regulated by PI3K/Akt, p53, AMP-activated protein kinase (AMPK) and MAPK/ERK1/2 pathways (52). Western blot analysis revealed

that mTOR signaling was decreased by the Akt pathway. Owing to the decreased total form of PI3K, the p-PI3K/PI3K ratio was not significantly decreased. However, the p-Akt/Akt ratio was decreased. It was concluded that mTOR signaling was affected by the Akt pathway.

Microtubule inhibitors, traditionally used as anticancer agents, remain a major therapy for numerous solid tumors, including numerous types of breast cancers. However, they have problems of drug resistance, neuropathy, immunosuppression and poor solubility. Currently, these problems have been overcome by changing the drug combination with chemotherapeutic drugs to reduce its toxicity and increase drug potency (53). In particular, the use of vincristine in cancer patients is dose-limited due to toxicity (54). While HDAC inhibitors are generally well-tolerated in humans, combining with vincristine may reduce the risk of toxicity to normal cells. Therefore, vincristine was used as a combination therapy with ACT-3 to determine its synergetic efficacy against MCF-7 cells. Cell cytotoxicity of the combination therapy showed the best effect with ACT-3 and vincristine. In previous studies, relatively high concentrations (>10 nM) of microtubule inhibitors have been shown to induce microtubule mass. However, a relatively low concentration (<10 nM) affects only the suppression of microtubule dynamics. This means that combination therapy with ACT-3 could reduce the side effects of vincristine while maintaining its anticancer effect (54,55). This synergetic effect could be explained briefly by the significant increase in p53 expression. As a result, apoptosis-related proteins, such as Bcl-2 and c-PARP, were also significantly increased. The autophagosome membrane protein LC3-II also greatly increased with the combination drug treatment. To date, numerous breast cancer chemotherapies have been developed; but alternative new drugs are required.

In conclusion, the present study aimed to determine the anticancer activity of ACT-3 in MCF-7 breast cancer cells. It was identified that ACT-3 inhibited cell proliferation and induced apoptosis and autophagic cell death via Akt/mTOR inhibition in MCF-7 cells. Moreover, combination therapy with traditional anticancer agents, including vincristine, showed a synergetic effect. Therefore, ACT-3 may be used alone or in combination with other anticancer drugs for the treatment of breast cancer.

Acknowledgements

Not applicable.

Funding

The present study was supported by the National Research Foundation (NRF) of Korea (grant nos. NRF-2019R1A2C2002923, NRF-2022R1A4A1018930 and 2021R1A2C1014595), funded by the Korean government.

Availability of data and materials

The datasets generated and/or analyzed during the current study are available from the corresponding author on reasonable request.

Authors' contributions

JSL and HSK conceived and designed the experiments. JSL and SYK performed the experiments. YJ and SYK separated and isolated the small molecules. JSL and JHK collected the data. JSL and HSK analyzed and interpreted the data and wrote the manuscript. ISK, JHK and HSK made critical revisions to the manuscript and confirm the authenticity of all the raw data. All authors have read and approved the final manuscript.

Ethics approval and consent to participate

Not applicable.

Patient consent for publication

Not applicable.

Competing interests

The authors declare that they have no competing interests.

References

1. Pojani E and Barlocco D: Romidepsin (FK228), A histone deacetylase inhibitor and its analogues in cancer chemotherapy. Curr Med Chem 28: 1290-1303, 2021.
2. West AC and Johnstone RW: New and emerging HDAC inhibitors for cancer treatment. J Clin Invest 124: 30-39, 2014.
3. Bass AKA, El-Zoghbi MS, Nageeb EM, Mohamed MFA, Badr M and Abuo-Rahma GEA: Comprehensive review for anticancer hybridized multitargeting HDAC inhibitors. Eur J Med Chem 209: 112904, 2021.
4. Sanaei M and Kavoosi F: Histone deacetylases and histone deacetylase inhibitors: Molecular mechanisms of action in various cancers. Adv Biomed Res 8: 63, 2019.
5. Ediriweera MK, Tennekoon KH and Samarakoon SR: Emerging role of histone deacetylase inhibitors as anti-breast-cancer agents. Drug Discov Today 24: 685-702, 2019.
6. Hanikoglu A, Hanikoglu F and Ozben T: Natural product inhibitors of histone deacetylases as new anticancer agents. Curr Protein Pept Sci 19: 333-340, 2018.
7. Wawruszak A, Kalafut J, Okon E, Czapinski J, Halasa M, Przybyszewska A, Miziak P, Okla K, Rivero-Muller A and Stepulak A: Histone deacetylase inhibitors and phenotypical transformation of cancer cells. Cancers (Basel) 11: 148, 2019.
8. Dawood M, Fleischer E, Klinger A, Bringmann G, Shan L and Efferth T: Inhibition of cell migration and induction of apoptosis by a novel class II histone deacetylase inhibitor, MCC2344. Pharmacol Res 160: 105076, 2020.
9. Suraweera A, O'Byrne KJ and Richard DJ: Combination therapy with histone deacetylase inhibitors (HDACi) for the treatment of cancer: Achieving the full therapeutic potential of HDACi. Front Oncol 8: 92, 2018.
10. Mottamal M, Zheng S, Huang TL and Wang G: Histone deacetylase inhibitors in clinical studies as templates for new anticancer agents. Molecules 20: 3898-3941, 2015.
11. Chen R, Zhang M, Zhou Y, Guo W, Yi M, Zhang Z, Ding Y and Wang Y: The application of histone deacetylases inhibitors in glioblastoma. J Exp Clin Cancer Res 39: 138, 2020.
12. Momenimovahed Z and Salehiniya H: Epidemiological characteristics of and risk factors for breast cancer in the world. Breast Cancer (Dove Med Press) 11: 151-164, 2019.
13. Damaskos C, Garmpis N, Valsami S, Kontos M, Spartalis E, Kalampokas T, Kalampokas E, Athanasiou A, Moris D, Daskalopoulou A, *et al*: Histone deacetylase inhibitors: An attractive therapeutic strategy against breast cancer. Anticancer Res 37: 35-46, 2017.
14. Naimo GD, Gelsomino L, Catalano S, Mauro L and Andò S: Interfering role of ERα on adiponectin action in breast cancer. Front Endocrinol (Lausanne) 11: 66, 2020.

15. Li J, Zhang T, Yang F, He Y, Dai F, Gao D, Chen Y, Liu M and Yi Z: Inhibition of breast cancer progression by a novel histone deacetylase inhibitor, LW479, by down-regulating EGFR expression. Br J Pharmacol 172: 3817-3830, 2015.
16. Newman DJ and Cragg GM: Natural products as sources of new drugs over the last 25 years. J Nat Prod 70: 461-477, 2007.
17. Connolly JD and Hill RA: Triterpenoids. Nat Prod Rep 24: 465-486, 2007.
18. Dzubak P, Hajduch M, Vydra D, Hustova A, Kvasnica M, Biedermann D, Markova L, Urban M and Sarek J: Pharmacological activities of natural triterpenoids and their therapeutic implications. Nat Prod Rep 23: 394-411, 2006.
19. Na M, Min BS, An RB, Jin W, Kim YH, Song KS, Seong YH and Bae K: Effect of the rhizomes of *Astilbe chinensis* on UVB-induced inflammatory response. Phytother Res 18: 1000-1004, 2004.
20. Sun HX, Ye YP and Pan YJ: Cytotoxic oleanane triterpenoids from the rhizomes of *Astilbe chinensis* (Maxim.) Franch. et Savat. J Ethnopharmacol 90: 261-265, 2004.
21. Hu JY, Yao Z, Xu YQ, Takaishi Y and Duan HQ: Triterpenes from *Astilbe chinensis*. J Asian Nat Prod Res 11: 236-242, 2009.
22. Tae IH, Son JY, Lee SH, Ahn MY, Yoon K, Yoon S, Moon HR and Kim HS: A new SIRT1 inhibitor, MHY2245, induces autophagy and inhibits energy metabolism via PKM2/mTOR pathway in human ovarian cancer cells. Int J Biol Sci 16: 1901-1916, 2020.
23. Ding J, Liu J, Zhang Z, Guo J, Cheng M, Wan Y, Wang R, Fang Y, Guan Z, Jin Y and Xie SS: Design, synthesis and biological evaluation of coumarin-based N-hydroxycinnamamide derivatives as novel histone deacetylase inhibitors with anticancer activities. Bioorg Chem 101: 104023, 2020.
24. Li Y and Seto E: HDACs and HDAC inhibitors in cancer development and therapy. Cold Spring Harb Perspect Med 6: a026831, 2016.
25. Li Y, Yuan YY, Meeran SM and Tollefsbol TO: Synergistic epigenetic reactivation of estrogen receptor-α (ERα) by combined green tea polyphenol and histone deacetylase inhibitor in ERα-negative breast cancer cells. Mol Cancer 9: 274, 2010.
26. Millot C, Millot JM, Morjani H, Desplaces A and Manfait M: Characterization of acidic vesicles in multidrug-resistant and sensitive cancer cells by acridine orange staining and confocal microspectrofluorometry. J Histochem Cytochem 45: 1255-1264, 1997.
27. Dong C, Wu J, Chen Y, Nie J and Chen C: Activation of PI3K/AKT/mTOR pathway causes drug resistance in breast cancer. Front Pharmacol 12: 628690, 2021.
28. Cras A, Darsin-Bettinger D, Balitrand N, Cassinat B, Soulié A, Toubert ME, Delva L and Chomienne C: Epigenetic patterns of the retinoic acid receptor beta2 promoter in retinoic acid-resistant thyroid cancer cells. Oncogene 26: 4018-4024, 2007.
29. Godman CA, Joshi R, Tierney BR, Greenspan E, Rasmussen TP, Wang HW, Shin DG, Rosenberg DW and Giardina C: HDAC3 impacts multiple oncogenic pathways in colon cancer cells with effects on Wnt and vitamin D signaling. Cancer Biol Ther 7: 1570-1580, 2008.
30. Zhang XH, Wang Z, Kang BG, Hwang SH, Lee JY, Lim SS and Huang B: Antiobesity effect of *Astilbe chinensis* Franch. et Savet. Extract through regulation of adipogenesis and AMP-activated protein kinase pathways in 3T3-L1 adipocyte and high-fat diet-induced C57BL/6N obese mice. Evid Based Complement Alternat Med 2018: 1347612, 2018.
31. Sancheti S, Sancheti S, Lee SH, Lee JE and Seo SY: Screening of Korean medicinal plant extracts for α-glucosidase inhibitory activities. Iran J Pharm Res 10: 261-264, 2011.
32. Gil TY, Jin BR, Hong CH, Park JH and An HJ: *Astilbe chinensis* ethanol extract suppresses inflammation in macrophages via NF-κB pathway. BMC Complement Med Ther 20: 302, 2020.
33. Zhang YB, Ye YP, Wu XD and Sun HX: Astilbotriterpenic acid induces growth arrest and apoptosis in HeLa cells through mitochondria-related pathways and reactive oxygen species (ROS) production. Chem Biodivers 6: 218-230, 2009.
34. Häcker G: The morphology of apoptosis. Cell Tissue Res 301: 5-17, 2000.
35. Zeiss CJ: The apoptosis-necrosis continuum: Insights from genetically altered mice. Vet Pathol 40: 481-495, 2003.
36. Vermeulen K, Van Bockstaele DR and Berneman ZN: The cell cycle: A review of regulation, deregulation and therapeutic targets in cancer. Cell Prolif 36: 131-149, 2003.
37. Nigg EA: Cyclin-dependent protein kinases: Key regulators of the eukaryotic cell cycle. Bioessays 17: 471-480, 1995.
38. Malumbres M and Barbacid M: Cell cycle, CDKs and cancer: A changing paradigm. Nat Rev Cancer 9: 153-166, 2009.
39. Satyanarayana A and Kaldis P: Mammalian cell-cycle regulation: Several Cdks, numerous cyclins and diverse compensatory mechanisms. Oncogene 28: 2925-2939, 2009.
40. Sauer K and Lehner CF: The role of cyclin E in the regulation of entry into S phase. Prog Cell Cycle Res 1: 125-139, 1995.
41. Peter M: The regulation of cyclin-dependent kinase inhibitors (CKIs). Prog Cell Cycle Res 3: 99-108, 1997.
42. Elmore S: Apoptosis: A review of programmed cell death. Toxicol Pathol 35: 495-516, 2007.
43. Hengartner MO: The biochemistry of apoptosis. Nature 407: 770-776, 2000.
44. Miyashita T, Krajewski S, Krajewska M, Wang HG, Lin HK, Liebermann DA, Hoffman B and Reed JC: Tumor suppressor p53 is a regulator of bcl-2 and bax gene expression in vitro and in vivo. Oncogene 9: 1799-1805, 1994.
45. Vaux DL, Cory S and Adams JM: Bcl-2 gene promotes haemopoietic cell survival and cooperates with c-myc to immortalize pre-B cells. Nature 335: 440-442, 1988.
46. Pietenpol JA and Stewart ZA: Cell cycle checkpoint signaling: Cell cycle arrest versus apoptosis. Toxicology 181-182: 475-481, 2002.
47. Beneke R, Geisen C, Zevnik B, Bauch T, Müller WU, Küpper JH and Möröy T: DNA excision repair and DNA damage-induced apoptosis are linked to Poly(ADP-ribosyl)ation but have different requirements for p53. Mol Cell Biol 20: 6695-6703, 2000.
48. Galluzzi L and Green DR: Autophagy-independent functions of the autophagy machinery. Cell 177: 1682-1699, 2019.
49. Apel A, Herr I, Schwarz H, Rodemann HP and Mayer A: Blocked autophagy sensitizes resistant carcinoma cells to radiation therapy. Cancer Res 68: 1485-1494, 2008.
50. Döring T, Zeyen L, Bartusch C and Prange R: Hepatitis B virus subverts the autophagy elongation complex Atg5-12/16L1 and does not require Atg8/LC3 lipidation for viral maturation. J Virol 92: e01513-e01517, 2018.
51. Li F, Guo H, Yang Y, Feng M, Liu B, Ren X and Zhou H: Autophagy modulation in bladder cancer development and treatment (review). Oncol Rep 42: 1647-1655, 2019.
52. Perez EA: Microtubule inhibitors: Differentiating tubulin-inhibiting agents based on mechanisms of action, clinical activity, and resistance. Mol Cancer Ther 8: 2086-2095, 2009.
53. Dumontet C and Jordan MA: Microtubule-binding agents: A dynamic field of cancer therapeutics. Nat Rev Drug Discov 9: 790-803, 2010.
54. Jordan VC: Chemoprevention of breast cancer with selective oestrogen-receptor modulators. Nat Rev Cancer 7: 46-53, 2007.
55. Younis AM, Wu FS and El Shikh HH: Antimicrobial activity of extracts of the oyster culinary medicinal mushroom Pleurotus ostreatus (higher basidiomycetes) and identification of a new antimicrobial compound. Int J Med Mushrooms 17: 579-590, 2015.